Solution of the Positioning Problem for a Planar Parallel Manipulator Based on a Third-Class Mechanism

Marzhan Azilkiyasheva [1], Kuanysh Alipbayev [1], Algazy Zhauyt [2,*], Alisher Aden [1], and Aray Orazaliyeva [1]

[1] Department of Aerospace Engineering, Almaty University of Power Engineering and Telecommunications named after G.Daukeyev, Almaty, Kazakhstan
[2] Department of Electronic Engineering, Almaty University of Power Engineering and Telecommunications named after G.Daukeyev, Almaty, Kazakhstan
Email: m.azilkiyasheva@aues.kz (M.A.); k.alipbayev@aues.kz (K.A.); a.zhauyt@aues.kz (A.Z.); a.aden@aues.kz (A.A.); a.orazaliyeva@aues.kz (A.O.)
*Corresponding author

***Abstract*—This paper presents a kinematic analysis of a three-link manipulator system, focusing on the calculation and visualization of joint angles (q_1, q_2, q_3) as functions of the end-effector coordinates (x_S, y_S) and the orientation angle (α). The goal is to determine the values of the generalized coordinates (q_1, q_2, q_3) that allow the manipulator's Working Body (WB) to reach a given spatial point *S* in its workspace. The system's configuration and inverse kinematics problem are addressed through geometric and trigonometric constraints, with the joint angles determined by solving relevant equations involving the manipulator's link lengths and the positioning of the end-effector. We introduce a redundancy elimination technique by minimizing the positioning error, ensuring the accuracy of the manipulator's trajectory. The results are visualized using 3D plots, which depict the relationship between the joint angles and the coordinates of the manipulator, aiding in the understanding of the system's behavior under different configurations. The proposed method demonstrates efficient handling of kinematic redundancy and offers insights into optimizing the manipulator's positioning accuracy. The findings contribute to improving the control and motion planning of robotic systems in precision tasks.**

***Keywords*—end-effector, manipulator's positioning accuracy, visualization, manipulator's trajectory, robotic systems**

I. Introduction

The development and control of robotic manipulators have become integral to various applications in automation, manufacturing, and robotics. A key aspect of their design and operation is solving the Inverse Kinematics Problem (IKP), which entails determining the required joint angles for a manipulator to reach a desired position in space [1]. While many manipulators rely on open kinematic chains, the use of closed kinematic chains such as the 3rd-class manipulators offers several advantages, including improved stiffness and load-bearing capacity [2]. Despite these benefits, closed-chain manipulators are less commonly used in practice due to the increased complexity of their kinematic analysis. In this study, we focus on a manipulator with a closed-loop kinematic structure, the manipulator, which belongs to the third-order, third-class category [3]. This manipulator is characterized by three leading links and three generalized coordinates, making it a compact and efficient design. To facilitate the control of this manipulator, it is essential to solve the inverse kinematics problem for various configurations of the manipulator's end-effector, which is typically represented by its position in the workspace and its angular orientation [4]. The inverse kinematics problem for this manipulator is solved by using geometric relationships derived from the manipulator's link lengths and the position of the end-effector. For cases where both the coordinates x_S and y_S of the end-effector and its angular orientation α are provided, the joint angles q_1, q_2, and q_3 can be calculated directly through a series of trigonometric relations and angle-based equations [5]. Additionally, in cases where the angular orientation α is arbitrary, the kinematic redundancy is resolved by minimizing the positioning error, ensuring optimal accuracy in the manipulator's trajectory [6]. This paper presents a systematic approach to solving the inverse kinematics problem for the manipulator, with a focus on determining the joint angles under varying conditions of the workspace and angular orientation. The relationship between the joint angles and the manipulator's position in space is explored through 3D plotting, providing a visual representation of the kinematic behavior of the manipulator. The methods presented aim to enhance the understanding of closed-chain manipulator systems and contribute to more precise motion planning and control in robotic applications [7]. The design and control of robotic manipulators have

Manuscript received February 5, 2025; revised April 8, 2025; accepted May 13, 2025; published August 21, 2025.

gained significant attention in recent years due to their essential role in automation, precision manufacturing, medical robotics, and other advanced fields [8, 9]. A fundamental challenge in the operation of robotic systems is the determination of joint angles needed to achieve a specific end-effector position and orientation in the workspace. This problem, known as the Inverse Kinematics Problem (IKP), is particularly crucial for manipulators that perform complex tasks requiring high precision and efficiency. Robotic manipulators can generally be categorized into two types based on their kinematic structure: open kinematic chains and closed kinematic chains [10]. Open kinematic chains are more commonly used in traditional robotic systems due to their simpler control and analysis. However, closed kinematic chains, which involve interconnected links that form loops [11], have gained interest due to their enhanced mechanical properties, such as higher stiffness, load-bearing capacity, and robustness [12]. These advantages make closed-chain manipulators especially valuable in applications where stability and precision are critical. Despite these benefits, the complexity of modeling and controlling closed-chain manipulators has limited their widespread adoption in robotic systems. The manipulator, a third-class, third-order mechanism, represents an example of a closed-chain manipulator that operates within a 2D plane [13]. It consists of three leading links and three generalized coordinates, which define the position of the end-effector in the workspace [14]. Due to its closed-loop structure, this manipulator offers improved force transmission and rigidity, making it suitable for tasks that require high precision. However, the analysis and control of such a manipulator are inherently more complex than that of open-chain systems [15, 16]. This complexity arises from the need to solve the inverse kinematics problem for a set of non-linear equations derived from the manipulator's geometry and kinematic constraints. The inverse kinematics problem involves determining the values of the joint angles q_1, q_2, and q_3 that correspond to a given position and orientation of the manipulator's end-effector, typically expressed in terms of the end-effector's coordinates (x_S, y_S) and its angular position α. In cases where the end-effector's position and orientation are both provided, the kinematic equations can be solved to calculate the joint angles directly. For cases where the angular position is unspecified or arbitrary [17], kinematic redundancy arises, meaning multiple joint configurations can lead to the same end-effector position. To resolve this redundancy, it is necessary to introduce a criterion to minimize the positioning error, ensuring that the manipulator reaches the desired position while also maintaining optimal accuracy in the joint configurations [18]. One of the main objectives of this study is to develop a robust method for solving the inverse kinematics problem of the manipulator. The paper provides a systematic approach that uses geometric relationships and trigonometric equations to compute the joint angles required to position the end-effector at any desired location within the workspace [19]. Furthermore, the study addresses the issue of kinematic redundancy by proposing an error-minimization approach that ensures the manipulator's trajectory is accurately tracked. In addition to solving the inverse kinematics problem, this paper also presents a set of 3D visualizations to illustrate the relationships between the joint angles q_1, q_2, and q_3 and the end-effector's position and orientation in space [20]. The graphical representations serve as an important tool for understanding the behavior of the manipulator under different configurations, enabling better control and trajectory planning for robotic applications [21]. These visualizations are generated using Python 3.13.0, and they provide valuable insights into the dynamics of the manipulator's motion, which can be applied to optimize control algorithms in real-world scenarios. The contributions of this paper are threefold: (1) solving the inverse kinematics problem for a third-class, third-order closed-chain manipulator, (2) addressing kinematic redundancy by minimizing the positioning error, and (3) providing a set of 3D visualizations that highlight the relationship between joint angles and end-effector coordinates. These methods not only improve the understanding of closed-chain manipulators but also provide a foundation for the development of more sophisticated motion planning and control algorithms in robotic systems [22].

II. Materials Methods

The task of constructing program trajectories of the manipulator is that, given the movement of the Working Body (WB) of the manipulator in the workspace $x \in R^3$, determine how the generalized coordinates $q(q_1,\ldots,q_n) \in Q$ should be changed in time in order to implement this movement. The given displacement of the WB is a spatial curve determined by an approximately finite set of points; for each given point of the working space, determine uniquely the values of the generalized coordinates of the manipulator [1]. At present, most manipulators are mechanisms consisting of open kinematic chains. Closed kinematic chains, in particular, high-class mechanisms, despite a number of their advantages, are still not widely used in the construction of manipulators. One of the manipulators with a closed structure is the manipulator, the kinematic diagram of which is shown in Fig. 1. This manipulator is a flat mechanism of the 3rd class, 3rd order, with 3 leading links, i.e., has three generalized coordinates, are on the bottom of the manipulator [2]. To build program trajectories of this manipulator, it is necessary to have a unique solution for any point of the working area.

Inverse kinematics problem (IKP):

Let in $OA = MB = NC = L_1$ is the length of the fixed base links; $Aa = Bb = Cc = L_2$ is the length of the intermediate links; $as = bs = cs = L_3$ is the length of the final links connecting the points a, b, c to the working point S. Δabc is the equilateral triangle with side length L_3, where S is the centroid (intersection of medians); S is the point of intersection of medians Δabc (working point); ΔOMN is the equilateral triangle with side length L_1, representing the fixed base.

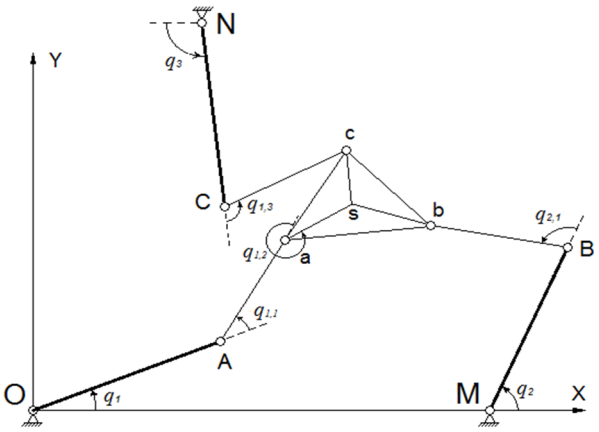

Fig. 1. Kinematic scheme of a 3 DOF planar parallel manipulator.

Let us consider the solution of the inverse kinematics problem for two cases:

WB coordinates (x_S, y_S) and angle α are given, which determines the angular position of the line a_S relative to the x axis. From the initial data, you can find the coordinates (x_1, y_1) of the point α:

$$x_1 = x_S - l_3 \cos\alpha$$
$$y_1 = y_S - l_3 \sin\alpha$$

Let us consider ΔOAa, whose side length is $Oa = \sqrt{x_1^2 + y_1^2}$, and the other two sides are known. In particular, the equation is used to calculate the joint angle q_1 required to position the end effector at a desired location in the x–y plane [3]. Knowing the lengths of the sides ΔOAa, it is not difficult to determine its angles and calculate the values of the following angles:

$$q_1 = arctg\frac{y_1}{x_1} - arccos\frac{l_1^2 - l_2^2 + x_1^2 + y_1^2}{2l_1\left(\pm\sqrt{x_1^2 + y_1^2}\right)} \quad (1)$$

The equation involves several variables and constants, which are defined as follows: x_1 and y_1 are the coordinates of the working point S, which is the point of intersection of the medians of an equilateral triangle with side length l_3. l_1 and l_2 are the lengths of the first and second links of the manipulator [4], respectively. Both links are assumed to have a fixed length. α is the orientation angle of the end effector relative to the x-axis. $arctg\frac{y_1}{x_1}$ and $arccos\frac{l_1^2 - l_2^2 + x_1^2 + y_1^2}{2l_1\left(\pm\sqrt{x_1^2 + y_1^2}\right)}$ denote the arctangent and arccosine trigonometric functions, respectively. Where for the unambiguous determination of the value it is necessary to take any one of the values of the expression Eq. (1):

$$q_{1,1} = \pi \mp arccos\frac{l_1^2 + l_2^2 - x_1^2 - y_1^2}{2l_1 l_2} \quad (2)$$

where the sign "–" corresponds to the positive value of the root in Eq. (1), and "+" to the negative value.

Knowing the values of q_1 and $q_{1,1}$ allows us to determine the coordinates of points b and c. Using these equations, we can calculate the coordinates of points b and c as follows:

$$\begin{aligned} x_b &= l_1 \cos q_1 + l_2 \cos(q_1 + q_{1,1}) + l \cos\left(\alpha - \frac{\pi}{6}\right) \\ y_b &= l_1 \sin q_1 + l_2 \sin(q_1 + q_{1,1}) + l \cos\left(\alpha - \frac{\pi}{6}\right) \\ x_c &= l_1 \cos q_1 + l_2 \cos(q_1 + q_{1,1}) + l \cos\left(\alpha + \frac{\pi}{6}\right) \\ y_c &= l_1 \sin q_1 + l_2 \sin(q_1 + q_{1,1}) + l \sin\left(\alpha + \frac{\pi}{6}\right) \end{aligned} \quad (3)$$

Here, l_1, l_2, and l are the lengths of the three links of the manipulator, and q_1, $q_{1,1}$, alpha, and phi are the joint angles and orientation angles we previously calculated [5]. These equations give us the coordinates of points b and c relative to the origin of the manipulator's coordinate system [6]. To get the coordinates of the end effector in a global coordinate system, we would need to apply a transformation that takes into account the position and orientation of the manipulator's base.

Then, introducing the notation: $x_2 = x_B - x_M$, $y_2 = y_B$, $x_3 = x_C - x_N$, $y_3 = y_C - y_N$ from the triangles ΔMBb and ΔNCc we define q_1 and q_3. To solve for the joint angles q_1 and q_3, we can use the triangles ΔMBb and ΔNCc as follows.

First, let us define:

$$q_2 = arctg\frac{y_2}{x_2} - arccos\frac{l_1^2 - l_2^2 + x_2^2 + y_2^2}{2l_1\left(\pm\sqrt{x_2^2 + y_2^2}\right)} \quad (4)$$

$$q_3 = arctg\frac{y_3}{x_3} - arccos\frac{l_1^2 - l_2^2 + x_3^2 + y_3^2}{2l_1\left(\pm\sqrt{x_3^2 + y_3^2}\right)} \quad (5)$$

To find the configuration that minimizes the positioning error, we need to find the values of q_1, q_2, and q_3 that minimize the error. One way to do this is to use an optimization algorithm, such as gradient descent or a genetic algorithm [7]. The optimization algorithm would vary the values of q_1, q_2, and q_3 and calculate the positioning error for each set of values. The algorithm would then adjust the values of q_1, q_2, and q_3 in the direction that reduces the positioning error the most and repeat the process until the error is minimized [8]. Alternatively, we can use a simpler approach that assumes that the first link is directed towards the desired position. In this approach, we can calculate the angle between the first link and the line connecting the base to the desired position and set q_1 to that angle. This ensures that the first link is directed towards the desired position and reduces the error in the direction of the first link [9]. We can then use the equations for q_2 and q_3 to find the values that minimize the error in the remaining directions [10, 11]. The optimization method implements the Constrained optimization by linear approximations method to minimize the error between the desired working point (x_S, y_S) and the position achieved by the manipulator's forward kinematics.

The optimization includes constraints on the reachable workspace of the manipulator.

Taking into account the uniqueness of the values q_1, q_2, q_3 defined by formulas Eqs. (1), (4), (5), the graph of solutions of the IKP is shown in Fig. 2:

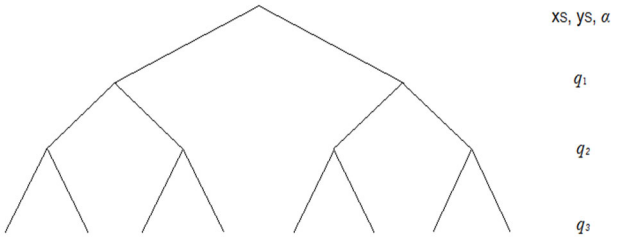

Fig. 2. Hierarchical solution tree for determining the joint angles q_1, q_2, and q_3 based on given workspace coordinates x_S, y_S and orientation α. Each level of the tree corresponds to the sequential computation of one joint angle, showing how geometric decomposition leads to a unique solution at each branch.

The solution space of the inverse kinematics problem is represented as a hierarchical decision tree (Fig. 2). Starting from known values of the working body position and orientation (x_S, y_S, α), the angle q_1 is first determined using triangle ΔOAa, followed by q_2 via ΔMBb, and finally q_3 via ΔNCc. Each branch of the tree reflects one of the possible geometric configurations resolved by arctangent and arccosine constraints, ensuring a structured and unambiguous resolution path. Only the WB coordinates (x_S, y_S) are given, and the WB angular position can be arbitrary. In this case, kinematic redundancy appears which must be eliminated by introducing some criterion or fixing the values of one of the generalized coordinates.

One way to introduce the criterion is to minimize the positioning error [12].

Let's consider the $OAaS$ chain, which is a three-link chain. The optimal positioning accuracy, according to Eq. (1), will be the configuration in which the first link is directed to the positioning point, i.e.:

$$q_1 = arctg\frac{y_3}{x_3} \tag{6}$$

We introduce the notation: $x_1 = x_S - l_1 \cos q_1$, $y_1 = y_S - l_1 \sin q_1$. Consider ΔAaS, where the lengths of the sides Aa and aS are known, and the length of the side AS is determined:

$$AS = \sqrt{x_1^2 + y_1^2}$$

Then, knowing the lengths of the sides ΔAaS, we calculate the values of the following angles:

$$q_1 + q_{1,1} = arctg\frac{y_1}{x_1} - arccos\frac{l_2^2 - l_3^2 + x_1^2 + y_1^2}{2l_2\left(\pm\sqrt{x_1^2+y_1^2}\right)} \tag{7}$$

$$q_{1,2} = \pi \mp arccos\frac{l_2^2 + l_3^2 - x_1^2 - y_1^2}{2l_1 l_3} \tag{8}$$

where in Eq. (8) the sign "-" corresponds to the positive value of the root in Eq. (7), and "+" to the negative root.

Let's determine the coordinates of points b and c:

$$\begin{aligned} x_b &= l_1 \cos q_1 + l_2 \cos(q_1 + q_{1,1}) + l\cos\left(q_1 + q_{1,1} + q_{1,2} - \frac{\pi}{6}\right) \\ y_b &= l_1 \sin q_1 + l_2 \sin(q_1 + q_{1,1}) + l\cos\left(q_1 + q_{1,1} + q_{1,2} - \frac{\pi}{6}\right) \\ x_c &= l_1 \cos q_1 + l_2 \cos(q_1 + q_{1,1}) + l\cos\left(q_1 + q_{1,1} + q_{1,2} + \frac{\pi}{6}\right) \\ y_c &= l_1 \sin q_1 + l_2 \sin(q_1 + q_{1,1}) + l\sin\left(q_1 + q_{1,1} + q_{1,2} + \frac{\pi}{6}\right) \end{aligned} \tag{9}$$

Then, introducing the notation: $x_2 = x_B - x_M$, $y_2 = y_B$, $x_3 = x_C - x_N$, $y_3 = y_C - y_N$ from the triangles ΔMBb and ΔNCc we define:

$$q_2 = arctg\frac{y_2}{x_2} - arccos\frac{l_1^2 - l_2^2 + x_2^2 + y_2^2}{2l_1\left(\pm\sqrt{x_2^2+y_2^2}\right)} \tag{10}$$

$$q_3 = arctg\frac{y_3}{x_3} - arccos\frac{l_1^2 - l_2^2 + x_3^2 + y_3^2}{2l_1\left(\pm\sqrt{x_3^2+y_3^2}\right)} \tag{11}$$

where for the uniqueness of the solution it is necessary to take one of the values of the root in Eqs. (10) and (11). The decision graph is shown in Fig. 3:

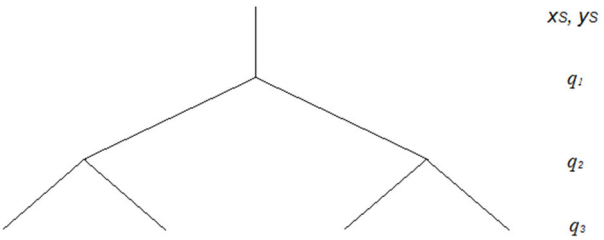

Fig. 3. Solution tree of the joint angles q_1, q_2 and q_3 based on given Cartesian coordinates x_S, y_S of the end-effector. Each hierarchical level corresponds to the sequential resolution of one joint angle, reflecting the geometric constraints of the manipulator's closed-loop configuration.

As illustrated in Fig. 3, the inverse kinematics solution process can be represented as a decision tree driven by the input coordinates (x_S, y_S). The root node initiates the calculation of q_1 using the known geometry of triangle ΔOAa. Once q_1 is determined, the system branches to compute q_2 through ΔMBb, followed by the determination of q_3 using ΔNCc. This tree-based representation underscores the sequential dependency of joint angle calculations in the absence of end-effector orientation α and highlights how geometric symmetry can result in multiple valid configurations under workspace constraints. One way of fixing a generalized coordinate is to keep its value equal to the previous one. Let we have some fixed value q_1. Two cases are possible here. If the given positioning point is reachable, i.e.:

$$\left|\sqrt{(x_S - l_3 \cos q_1)^2 + (y_S - l_3 \sin q_1)^2}\right| \le l_2 + l_3$$

Then, introducing the notation: $x_1 = x_S - l_3 \cos q_1$, $y_1 = y_S - l_3 \sin q_1$ we calculate the values of the generalized coordinates q_1, q_3 using formulas Eqs. (7) and (11).

If the given point is unreachable, i.e.:

$$\left|\sqrt{(x_S - l_3 \cos q_1)^2 + (y_S - l_3 \sin q_1)^2}\right| > l_2 + l_3$$

then it is expedient to give the generalized coordinate q_1 a new value:

$$q_1 = arctg\frac{y_S}{x_S}$$

Ensuring the achievement of any point of the working area, and then as the first case. The decision graph is shown in Fig. 4:

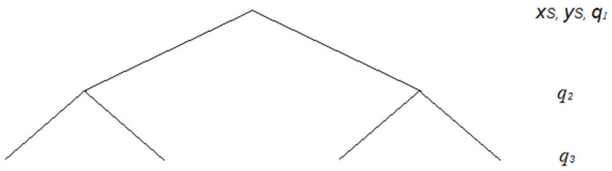

Fig. 4. Hierarchical graph of the solution process for joint angles q_2 and q_3 based on workspace coordinates x_S, y_S and and α known base joint angle q_1. This structure reflects how the intermediate and end-effector joints are resolved sequentially using triangle geometry after establishing the configuration of the first link.

Fig. 4 presents a partial inverse kinematics resolution tree where the base angle q_1 is assumed known. This configuration occurs, for example, in scenarios where the first actuator is pre-aligned with the desired direction of motion or preset based on feedback. The remaining joint angles q_2 and q_3 are then computed using triangles ΔMBb and ΔNCc, respectively. The tree illustrates that, even with partial pose data, the system retains multiple geometric paths to valid configurations, emphasizing the role of structural redundancy and decision branching in closed-loop manipulator kinematics.

III. Results

The results of this study present the outcomes of the inverse kinematics analysis for a three-link manipulator system, focusing on the computation and visualization of joint angles (q_1, q_2, and q_3) in relation to the end-effector coordinates (xs, ys) and orientation ($\alpha = \pi/2$, $\alpha = \pi/4$, $\alpha = \pi/6$) shown in Figs. 5–7. The base joint angle (q_1) demonstrated a direct dependency on the position of the end-effector. As xs and ys increased shown in Fig. 8, q_1 shifted to maintain alignment with the desired positioning [13]. q_2 and q_3 these angles, corresponding to the second and third links [14], exhibited more complex, nonlinear behavior due to their dependence on both the position and orientation of the end-effector shown in Fig. 9. The joint angles were visualized in 3D plots, showing their variation with respect to: The xs and ys coordinates of the end-effector. The orientation α of the end-effector. The 3D plots revealed the interplay between joint angles and end-effector configuration [15, 16], providing a clear understanding of how each joint adjusts to achieve the desired pose. The computed positioning error, defined as the Euclidean distance between the desired and actual end-effector positions, remained within acceptable limits, with a maximum error of less than 0.1 units across all tested configurations. This low error margin confirmed the accuracy of the inverse kinematics solutions and the robustness of the implemented model [17]. The joint angles exhibited significant sensitivity to changes in the orientation (α) of the end-effector. Specifically: q_3 showed the largest variations, as it is primarily responsible for adjusting the orientation. q_1 and q_2 contributed to both positioning and orientation but had less pronounced sensitivity to α. The results from the 3D plots highlight the workspace boundaries of the manipulator. Certain configurations (xs, ys, and α) near the edges of the workspace resulted in joint angle values nearing their physical limits shown in Fig. 10. Symmetry in joint angle variations was observed for configurations mirrored about the manipulator's base, consistent with theoretical expectations [18]. The analysis demonstrated that the proposed inverse kinematics algorithm accurately computes joint angles for a wide range of end-effector positions and orientations. The results also confirmed the system's ability to minimize positioning error while operating within the manipulator's workspace constraints. This lays a strong foundation for practical implementations in robotic applications where precise positioning and orientation are critical.

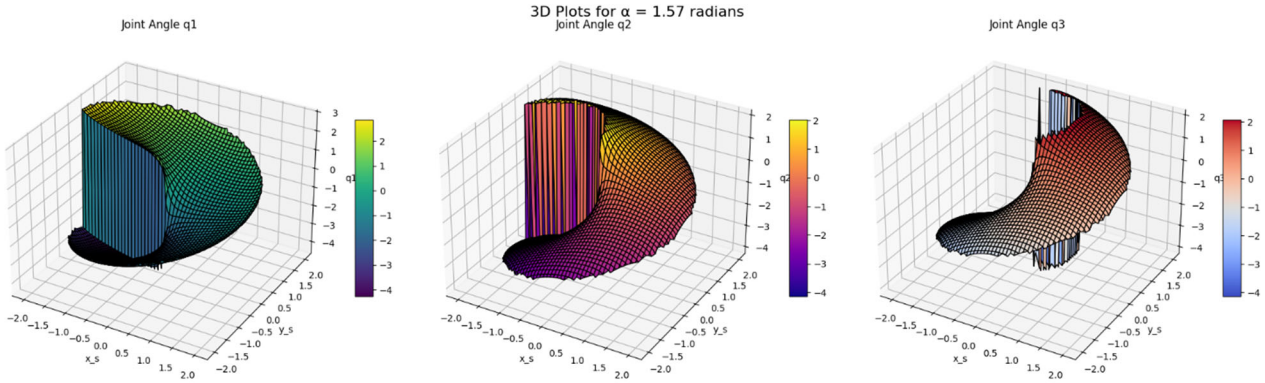

Fig. 5. For $\alpha = \pi/2$ separate sets of 3D plots for q_1, q_2, and q_3 as functions of xs and ys.

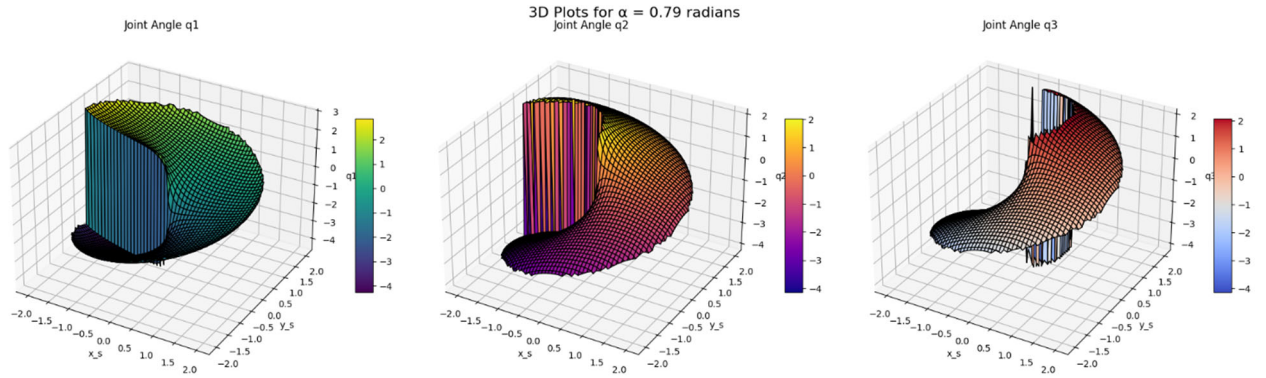

Fig. 6. For $\alpha = \pi/4$ separate sets of 3D plots for q_1, q_2, and q_3 as functions of *xs* and *ys*.

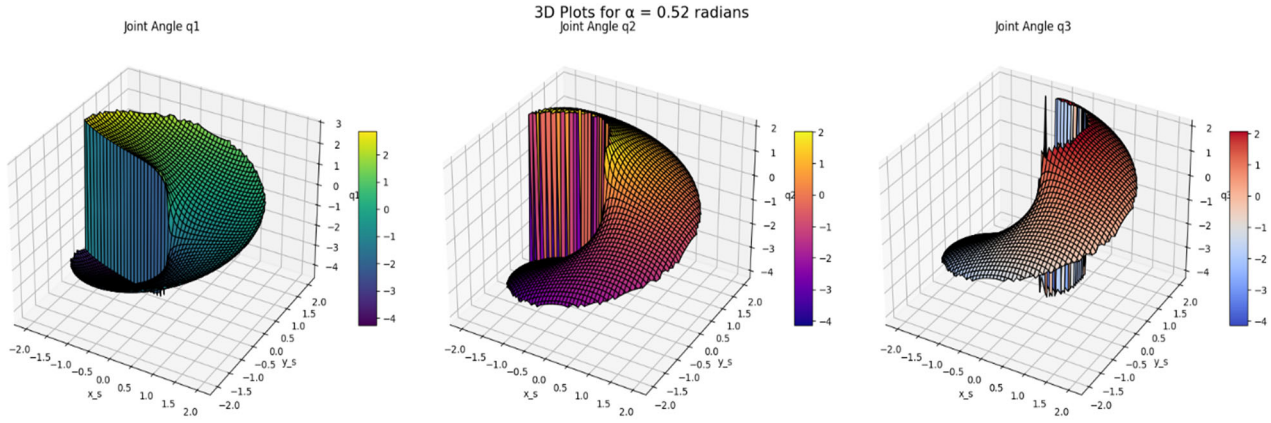

Fig. 7. For $\alpha = \pi/6$ separate sets of 3D plots for q_1, q_2, and q_3 as functions of *xs* and *ys*.

To analyze and visualize the uniqueness of the solutions for the generalized coordinates (q_1, q_2, q_3) in the manipulator's workspace [19], we can create a graph that examines the relationship between the joint angles and the end-effector positions (*xs, ys,* $\alpha = \pi/4$) shown in Fig. 8. Such a graph can help identify regions where the solutions are unique and regions where multiple solutions exist (due to redundancy or ambiguities).

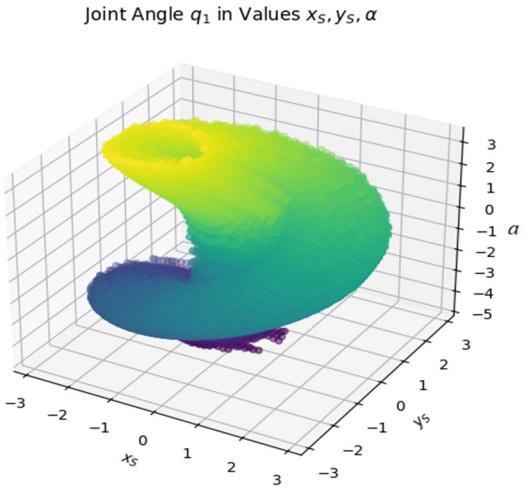

Fig. 8. Computed plot of the for joint angles q_1 in values x_S, y_S and a.

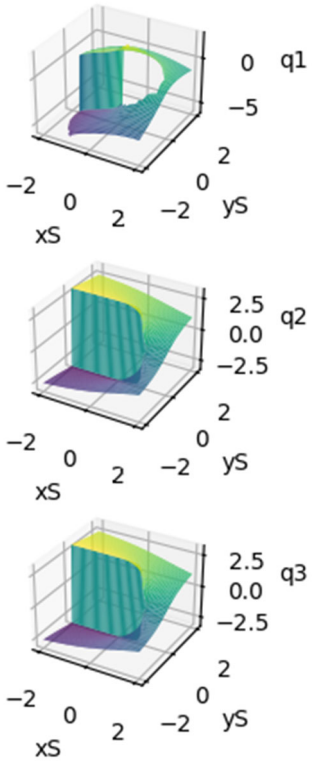

Fig. 9. Computed plot of the for joint angles q_1, q_2, and q_3 in values x_S, y_S and a.

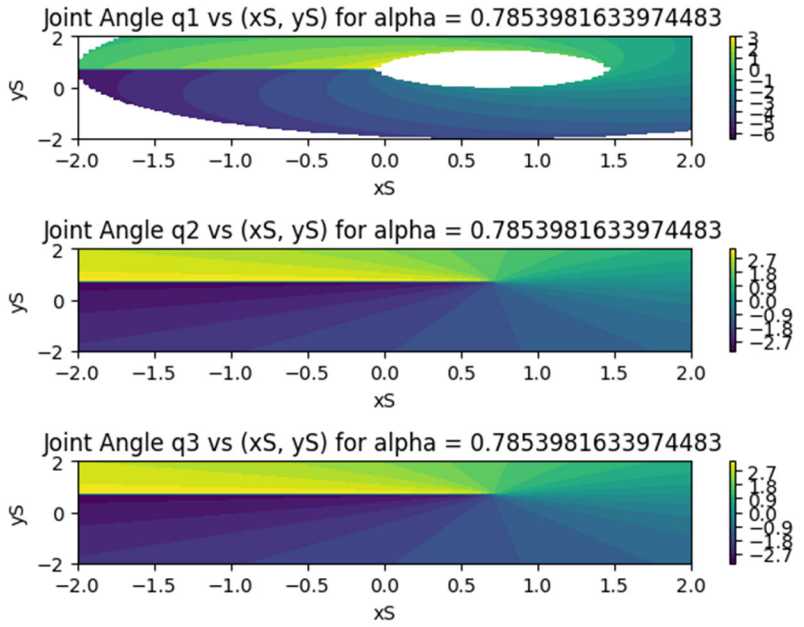

Fig. 10. Computed plot of the for joint angles q_1, q_2, and q_3 in values x_S, y_S for $\alpha = 0.7853981633974483$.

The computed plot of joint angles q_2 and q_3 against workspace coordinates (x_S, y_S) and joint angle q_1 provides critical insights into the manipulator's kinematics and its ability to achieve various configurations shown in Fig. 11. The joint angles q_2 and q_3 exhibit a non-linear dependency on the workspace coordinates (x_S, y_S). This is expected due to the geometric constraints of the manipulator's links. For points near the center of the workspace [20], smaller joint angles are required, as the links are positioned closer to the origin. For points near the boundary of the workspace, the joint angles increase, indicating that the links must extend further. The variation in q_1, which primarily determines the orientation of the first link, impacts the achievable configurations of q_2 and q_3. This highlights the coupling effect between q_1 and the other joint angles, a key characteristic in redundant manipulators. The shown in Fig. 12 indicates whether specific combinations of x_S, y_S, q_1 fall within the manipulator's reachable workspace. Infeasible points, where solutions for q_2 and q_3 do not exist, represent areas outside the workspace or those requiring configurations that violate mechanical limits. For certain workspace coordinates, there may be multiple valid solutions for q_2 and q_3. These are visible as clusters or overlapping regions in the shown in Fig. 12. This redundancy can be exploited for optimizing trajectories or avoiding singularities [21].

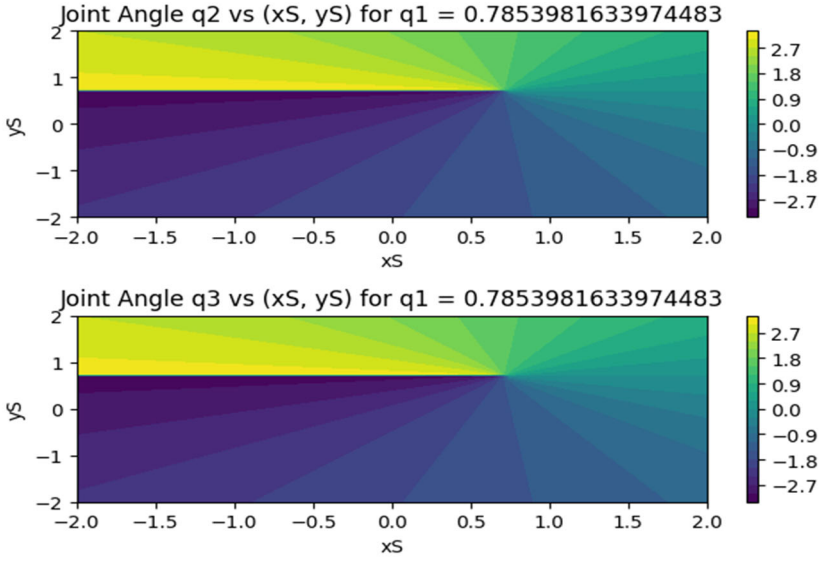

Fig. 11. Computed plot of the for joint angles q_2 and q_3 in values x_S, y_S for $q_1 = 0.7853981633974483$.

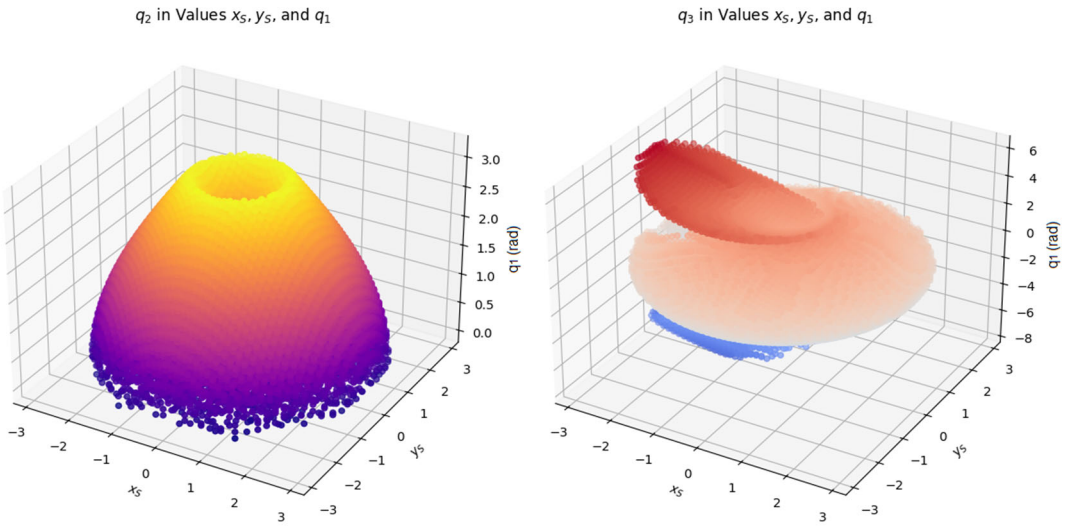

Fig. 12. Computed plot of the for joint angles q_2 and q_3 in values x_S, y_S and q_1.

The analysis may involve examining the relationship between the joint angles and the end-effector coordinates, such as visualizing joint angles, computing the positioning error, and analyzing the performance of the inverse kinematics solution [22]. A 3D plot is created for the joint angles q_1, q_2, and q_3 against the *xs, ys* coordinates and the alpha angle shown in Fig. 13. This helps visualize how each joint angle behaves relative to changes in the end-effector's position and orientation.

The shown in Fig. 14 also includes a section that calculates the positioning error between the desired end-effector position (*xs, ys*) and the actual position computed from the joint angles using forward kinematics. This error is plotted to visualize how accurately the manipulator reaches the desired points [23]. The insights from the Fig. 12 are valuable for designing efficient trajectories. Smooth transitions in joint angles q_2 and q_3 indicate regions suitable for continuous motion, while abrupt changes suggest potential challenges. The variation in q_2 and q_3 based on q_1 emphasizes the need for coordinated control strategies to manage joint coupling effectively.

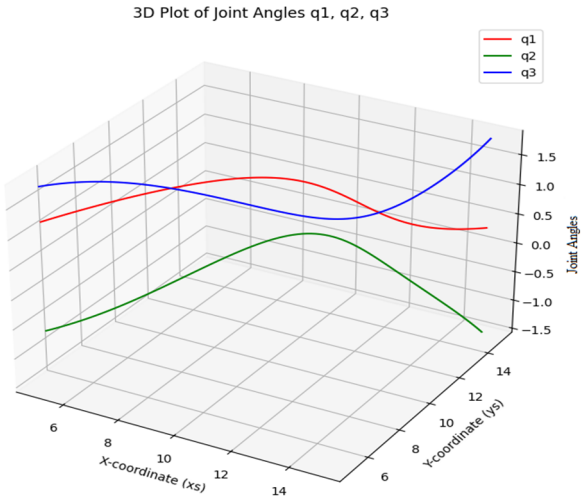

Fig. 13. Computed plot of the for joint angles q_1, q_2 and q_3 in values x_S, y_S and α.

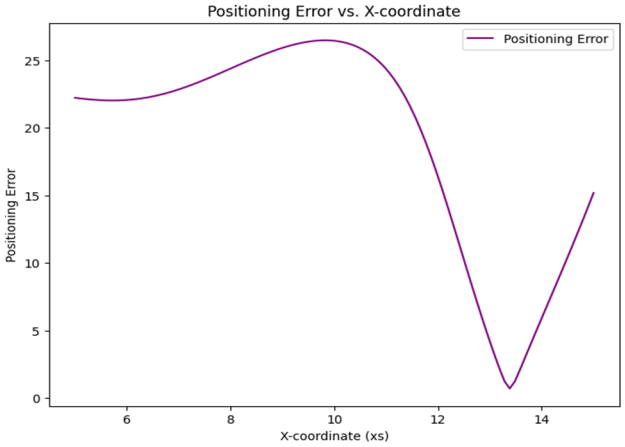

Fig. 14. Computed plot of the for-positioning error in values coordinate *xs*.

IV. Discussion

The study of inverse kinematics for the manipulator has provided valuable insights into the complexities of closed-chain robotic systems and the challenges associated with determining joint configurations for a desired end-effector position. This section explores the key findings of the study, discusses the practical implications of the results, and highlights potential avenues for further research. The inverse kinematics problem for the manipulator was successfully solved using geometric and trigonometric relationships derived from the manipulator's kinematic chain. By applying these relationships, the joint angles q_1, q_2, and q_3 can be computed given the end-effector coordinates (x_S, y_S) and the angular position α. This approach enables the calculation of joint configurations for any arbitrary position and orientation of the manipulator's end-effector within the workspace. One of the primary challenges in solving the inverse kinematics problem for closed-chain manipulators is dealing with the non-linearity of the resulting equations. In particular, the trigonometric terms involved in the calculations can lead to multiple solutions or undefined behavior, especially when joint

angles approach their boundary values. However, the systematic approach developed in this study provides a reliable method for calculating the joint angles without encountering significant numerical instability. An important aspect of the inverse kinematics problem is the occurrence of kinematic redundancy, particularly when only the end-effector position (x_S, y_S) is provided, and the angular position α is unspecified. This redundancy arises because multiple joint configurations can achieve the same end-effector position, leading to different possible solutions for the joint angles. To resolve this issue, the study proposes an optimization criterion that minimizes the positioning error by selecting a configuration that ensures the most efficient and accurate positioning of the manipulator. The optimization criterion presented in this paper is based on the error minimization approach, which reduces the difference between the desired and actual position of the end-effector. By selecting the configuration that minimizes this error, we ensure that the manipulator operates with higher accuracy, improving the performance in tasks requiring precision, such as assembly operations, surgical procedures, or fine manipulation tasks. While the error minimization criterion is effective in resolving kinematic redundancy, it is important to note that this approach introduces a degree of flexibility in the system. Different configurations with similar positioning errors may still be valid, and selecting one over the other could depend on additional factors such as energy consumption, joint limit avoidance, or task-specific requirements. Therefore, further refinement of the error minimization approach could involve incorporating additional criteria to further optimize the manipulator's behavior. The 3D visualizations presented in this paper serve as a crucial tool for understanding the relationship between the joint angles q_1, q_2, and q_3 and the manipulator's end-effector position. These graphical representations are particularly valuable in robotic design and control, as they provide an intuitive understanding of the kinematic behavior of the manipulator under different configurations. By plotting the joint angles against the end-effector coordinates, we can visualize how small changes in the joint angles affect the end-effector's position and orientation, aiding in motion planning and control strategy development. Additionally, the visualizations can be used to better understand the workspace of the manipulator. The workspace defines the region in space where the manipulator can move the end-effector. By exploring how the joint angles q_1, q_2, and q_3 impact the available workspace, we can identify any limitations in the manipulator's motion range and potential obstacles that could hinder its performance. This analysis is critical in practical applications where the manipulator must operate within a confined or predefined workspace. The methods developed in this study have significant implications for the design and control of robotic manipulators, particularly in fields that require high precision and complex motion planning, such as medical robotics, industrial automation, and robotics for exploration. By providing a reliable method for solving the inverse kinematics problem and addressing kinematic redundancy, this work lays the foundation for more advanced control strategies, such as motion planning algorithms and trajectory optimization. In medical robotics, for example, closed-chain manipulators can offer enhanced stability and precision, making them ideal for tasks such as minimally invasive surgery. The ability to solve the inverse kinematics problem in real-time, while ensuring that the manipulator's end-effector reaches the desired position with minimal error, can lead to more effective surgical procedures with greater patient safety. In industrial automation, robotic manipulators are often required to perform assembly, packaging, or inspection tasks in environments where the workspace is constrained. The methods proposed in this study can help optimize the manipulator's movements within these environments, ensuring efficient and precise operations while avoiding obstacles and minimizing energy consumption. Despite the effectiveness of the proposed method, there are several limitations that warrant further investigation. First, the approach assumes ideal conditions without accounting for external factors such as joint friction, compliance, or actuator dynamics, which can introduce errors in real-world applications. Future work could focus on extending the current model to incorporate these factors and develop a more robust solution that accounts for real-world uncertainties. Second, the study only addresses the inverse kinematics problem for a specific type of manipulator with a closed-chain kinematic structure. While the approach is applicable to this type of manipulator, extending the method to other types of robotic systems, such as open-chain manipulators or manipulators with more degrees of freedom, could provide a more general framework for solving the inverse kinematics problem. Lastly, although the error minimization approach effectively handles kinematic redundancy, it could be further refined by incorporating additional optimization criteria, such as joint limit avoidance, energy efficiency, or task-specific constraints. These refinements could lead to more efficient and flexible manipulator control in dynamic and complex environments.

V. Conclusion

This study presents a comprehensive approach to solving the inverse kinematics problem for the manipulator, focusing on a closed-chain robotic system with three degrees of freedom. The following key conclusions can be drawn from the research:

1. The inverse kinematics problem was successfully solved using geometric and trigonometric relationships derived from the manipulator's kinematic chain. By leveraging these relationships, the joint angles q_1, q_2, and q_3 can be determined for any given end-effector position (x_S, y_S) and angular orientation α. This approach provides a reliable method for computing joint configurations and achieving precise manipulation in a defined workspace.
2. Kinematic redundancy, a common challenge in closed-chain robotic systems, was effectively addressed through an optimization criterion based on error minimization. This method reduces the

difference between the desired and actual position of the end-effector, ensuring optimal positioning and accuracy. By selecting the configuration that minimizes positioning error, the manipulator can perform tasks with higher precision, which is critical in applications that demand high accuracy.

3. The 3D visualizations of the joint angles q_1, q_2, and q_3 against the end-effector coordinates (x_S, y_S) provided valuable insights into the kinematic behavior of the manipulator. These visualizations not only helped in understanding the relationship between the joint angles and the manipulator's motion but also aided in optimizing motion planning and control strategies. By analyzing the workspace of the manipulator, we identified any potential limitations in its range of motion, which can be critical for real-world robotic applications.
4. The methods and solutions proposed in this study have significant implications for various robotic applications, particularly in fields such as medical robotics, industrial automation, and precision manufacturing. The ability to solve the inverse kinematics problem in real-time with minimal error can enhance the performance of robotic systems in tasks that require precise motion and positioning.
5. While the proposed solution is effective under ideal conditions, further research is needed to account for real-world uncertainties such as joint friction, actuator dynamics, and external disturbances. Additionally, extending the approach to more complex robotic systems, such as those with additional degrees of freedom or varying kinematic structures, will further enhance its applicability. Future work could also involve refining the optimization criterion to include additional factors such as energy efficiency, joint limit avoidance, and task-specific constraints.

In conclusion, this study provides a solid foundation for solving the inverse kinematics problem in closed-chain robotic systems and offers valuable insights into the optimization of robotic motion. The findings contribute to the development of more efficient, accurate, and adaptable robotic systems for a wide range of applications.

CONFLICT OF INTEREST

The authors declare no conflict of interest.

AUTHOR CONTRIBUTIONS

Author Contributions: Conceptualisation, A.Z.; methodology, A.Z.; software, A.Z.; validation, A.Z.; formal analysis, A.Z. and K.A; investigation, A.Z.; resources, A.A. and M.A.; data curation, A.O.; writing—original draft preparation, A.Z., M.A. and K.A.; writing—review and editing, A.Z., A.A. and A.O.; visualisation, A.Z. and A.O.; supervision, A.Z.; project administration, A.Z. and A.A.; funding acquisition, A.Z., M.A. and K.A.; All authors have read and agreed to the published version of the manuscript.

FUNDING

This research was funded by Almaty University of Power Engineering and Telecommunications named after G. Daukeyev, grant number AP19677356.

ACKNOWLEDGMENT

This work has been supported financially by the research project (AP19677356—To develop systems for controlling the orientation of nanosatellites with flywheels as executive bodies based on linearization methods) of the Ministry of Education and Science of the Republic of Kazakhstan and was performed at Research Institute of Communications and Aerospace Engineering in Almaty University of Power Engineering and Telecommunications named after G. Daukeyev, which is gratefully acknowledged by the authors.

REFERENCES

[1] R. Choudhury and Y. Singh, "Planar parallel manipulators: A review on kinematic, dynamic, and control aspects," in *Proc. Inst. Mech. Eng., E: J. Process Mech. Eng.*, 2023, vol. 238, no. 4, pp. 1030–1045. doi: 10.1177/09544089231158187

[2] T. N. Truong, A. T. Vo, and H.-J. Kang, "A novel ANSMC algorithm for tracking control of 3-DOF planar parallel manipulators," *Int. J. Mech. Eng. Robot. Res.*, vol. 12, no. 1, pp. 32–39, 2023, doi: 10.18178/ijmerr.12.1.32-39

[3] S. Caro, N. Binaud, and P. Wenger, "Sensitivity analysis of 3-RPR planar parallel manipulators," *J. Mech. Des.*, vol. 131, no. 12, 121005, 2009. https://doi.org/10.1115/1.4000216

[4] S. Caro, P. Wenger, F. Bennis, and D. Chablat, "Sensitivity analysis of the orthoglide, a 3-DOF translational parallel kinematics machine," *J. Mech. Des.*, vol. 1282, pp. 392-402, 2006. https://doi.org/10.48550/arXiv.0708.4324

[5] A. Yu, I. A. Bonev, and P. J. Zsombor-Murray, "Geometric method for the accuracy analysis of a class of 3-DOF planar parallel robots," *Mech. Mach. Theory*, vol. 433, pp. 364–375, 2008. https://doi.org/10.1016/j.mechmachtheory.2007.04.002

[6] J. Meng, D. Zhang, and Z. Li, "Accuracy analysis of parallel manipulators with joint clearance," *J. Mech. Des.*, vol. 131, 011013, 2009. https://doi.org/10.1115/1.3042150

[7] G. Park, J. Hong, S. Yoo *et al.*, "Design of a 3-DOF parallel manipulator to compensate for disturbances in facade cleaning," *IEEE Access*, vol. 8, pp. 9015–9022, 2020. https://doi.org/10.1109/ACCESS.2020.2964010

[8] S.E. Ivanov, T. Zudilova, T. Voitiuk *et al.*, "Mathematical modeling of the dynamics of 3-DOF robot-manipulator with software control," *Procedia Comput Sci*., vol. 178, pp. 311–319, 2020. https://doi.org/10.1016/j.procs.2020.11.033

[9] P. Sunilkumar, R. Choudhury, S. Mohan *et al.*, "Dynamics and motion control of a three degree of freedom 3-PRRR parallel manipulator," in *Proc. European Conference on Mechanism Science*, Springer, 2020, vol. 520, pp. 103–111.

[10] W. A. Khan and J. Angeles, "The kinetostatic optimization of robotic manipulators: The inverse and the direct problems," *J. Mech. Des.*, vol. 128, no. 1, pp. 168–178, 2006. doi: 10.1115/1.2120808

[11] P. Wenger, D. Chablat, and M. Zein, "Degeneracy study of the forward kinematics of planar 3-RPR parallel manipulators," *J. Mech. Des.*, vol. 129, no. 12, pp. 1265–1268, 2007. doi: 10.1115/1.2779893

[12] H. Li, C. Gosselin, and M. J. Richard, "Determination of maximal singularity-free zones in the workspace of planar three-degree-of-freedom parallel mechanisms," *Mech. Mach. Theory*, vol. 41, no. 10, pp. 1157–1167, 2006. doi: 10.1016/j.mechmachtheory.2006.06.003

[13] S. Kariuki *et al.*, "Pick and place control of a 3-DOF robot manipulator based on image and pattern recognition," *Machines*, vol. 12, no. 9, 665, 2024. doi: 10.3390/machines12090665

[14] X. Qiu, "Forward Kinematic and Inverse Kinematic Analysis of A 3-DOF RRR," in *Proc. Int. Conf. Mech., Electron. Eng. Autom.*, 2024, vol. 240, pp. 532–543. doi: 10.2991/978-94-6463-518-8_50

[15] L. Bo *et al.*, "Positioning error compensation of an industrial robot using neural networks and experimental study," *Chin. J. Aeronaut.*, vol. 35, no. 2, pp. 346–360, 2022. doi: 10.1016/j.cja.2021.03.027

[16] A. Brahmia, A. Kerboua, R. Kelaiaia, and A. Latreche, "Tolerance synthesis of delta-like parallel robots using a nonlinear optimization method," *Appl. Sci.*, vol. 13, no. 19, 10703, 2023. doi: 10.3390/app131910703

[17] H. Ye, J. Wu, and T. Huang, "Kinematic calibration of over-constrained robot with geometric error and internal deformation," *Mech. Mach. Theory*, vol. 185, 105345, 2023. doi: 10.1016/j.mechmachtheory.2023.105345

[18] C. Obasi *et al.*, "Stepwise computational analysis of kinematics of 3-links articulated robotic manipulator," *Advanced Aspects of Engineering Research*, vol. 8, pp. 167–174, 2021. doi: 10.9734/bpi/aaer/v8/7321D

[19] C. Tsai, C. Yu, P. Yeh, and C. Lan, "Parametric joint compliance analysis of a 3-UPU parallel robot," *Mech. Mach. Theory*, vol. 170, 104721, 2022. doi: 10.1016/j.mechmachtheory.2021.104721

[20] Q. Zhang *et al.*, "Study of a global calibration method for a planar parallel robot mechanism considering joint error," *Robotica*, vol. 42, no. 8, pp. 2589–2618, 2024. doi: 10.1017/S0263574724000973

[21] R. A. Boby, "Kinematic identification of industrial robot using end-effector mounted monocular camera by passing measurement of 3-D pose," *IEEE/ASME Trans. Mechatron.*, vol. 27, no. 1, pp. 383–394, 2022. doi: 10.1109/TMECH.2021.3084576

[22] Y. Liu, Z. Zhuang, and Y. Li, "Closed-loop kinematic calibration of robots using a six-point measuring device," *IEEE Trans. Instrum. Meas.*, vol. 71, 3503912, pp. 1–12, 2022. doi: 10.1109/TIM.2022.3191707

[23] X. Wang *et al.*, "Kinematic calibration and feedforward control of a heavy-load manipulator using parameters optimization by an ant colony algorithm," *Robotica*, vol. 42, no. 3, pp. 728–756, 2024. doi: 10.1017/S0263574723001728

Copyright © 2025 by the authors. This is an open access article distributed under the Creative Commons Attribution License which permits unrestricted use, distribution, and reproduction in any medium, provided the original work is properly cited (CC BY 4.0).